EURASIAN PHYSICAL TECHNICAL JOURNAL

2024, Volume 21, No. 2 (48)

https://doi.org/10.31489/2024No2/38-48

Received: 14/11/2023 Revised: 16/02/2024 Accepted: 06/06/2024 Published online: 29/06/2024

Original Research Article

UDC 537.322

DIRECT CONTACT RESISTANCE MEASUREMENT DURING THERMOELECTRIC TESTING

Soldatov A.I.[1], Soldatov A.A.[1], Abouellail A.A.[2], Kostina M.A.[1]

[1] National Research Tomsk Polytechnical University, Tomsk, Russia,

[2] Sphinx University, New Asyut, Egypt

*Corresponding author: mariyakostina91@mail.ru

Abstract. *The article analyzes the influence of the contact resistance of the electrodes on the inspection result. It is shown that as the value of the measuring resistor increases, the permissible value of the contact resistance of the electrodes with the test sample increases. An indirect method for monitoring contact resistance has been proposed, which consists of passing a stable high-frequency current through the contact resistance and measuring the voltage across this resistance. The variation of relative voltage across the measuring resistor with respect to the total contact resistance has been graphed. The maximum allowable contact resistance has been determined to ensure that the measured thermoelectric EMF differs from the true value by no more than 10%. The proposed method allows to measure contact resistance directly in the process of monitoring thermoelectromotive force.*

Keywords: thermoelectromotive force, hot electrode, cold electrode, contact resistance, current generator, filter, measuring resistor.

1. Introduction

The thermoelectric method is widely used for rapid testing of metals and alloys [1, 2]. It allows to define the size of the decarburized layer and the quality of heat treatment, to sort supplied rolled metal and sort finished products by steel grade, to determine the thickness of the steel carburization layer, and to determine the amount of plastic deformation [3-12]. The thermoelectric dependence of X5CrNi18-10 stainless steel on the magnitude of plastic deformation was studied in [13], and the thermoelectric characteristics of plastically deformed steels ST3, 08KP AND 12H18N10T were studied in [14].

At the beginning of the 21st century, the thermoelectric method began to be used to test the temperature of the weld in the friction stir welding process, based on measuring the temperature with a thermocouple formed by the tool-workpiece connection [15-19]. The thermoelectric method was also used to control the thermal resistance of the cooling radiator-body of a power semiconductor element system [20]. Another area of application of the thermoelectric method is the measurement of the Seebeck coefficient of materials and alloys [21-23]. The thermoelectric method has been successfully applied to inspect the thermal resistance of a thermal interface and assess the degree of hydrogenation of a titanium alloy [24-27].

To solve problems of thermoelectric testing, several types of thermoelectric testing devices are currently commercially produced. The ACTTR company from Taiwan produces SETARAM SeebeckPro for Seebeck coefficient measurement. Linseis Messgeraete GmbH from Germany produces a line-up of Seebeck coefficient and electrical resistance devices: SR-1, SR-3, etc. NETZSCH from Germany produces SBA 458

NEMESIS for measuring Seebeck coefficient. The Japanese ULVAC GmbH produces “ZEM-3” for measuring thermoelectromotive force (thermoEMF) and the Seebeck coefficient. Russian companies produce OMET, METEK and T-3SP devices.

The time consumed by the thermoelectric method does not exceed 3-5 seconds, which is an advantage of this method. The small dimensions of thermoelectric flaw detectors and the simple testing technique are additional advantages of this method [28].

One of the disadvantages of thermoelectric inspection devices is the presence of contact resistance at the points of connection of the electrodes with the test sample. The magnitude of the contact resistance will depend on the force of pressing the electrodes to the sample, the angle of inclination of the sensor, and the distribution of the load over the area of the electrodes [29-30]. This is especially evident during manual testing, in which it is impossible to ensure the same pressing force and the same deviation of the electrodes between the normal and the test sample. In addition, the contact resistance will depend on the quality of preparation of the surface of the electrodes and the tested product, on the presence of an oxide film, etc. In particular, in it is noted that upon the presence of an oil film on the surface of the electrodes or the test product, the contact resistance can increase to 100 Ω and higher. The influence of contact resistance on the thermoEMF value was studied in [31]. The authors proposed a way to reduce the contact resistance, which led to a decrease in the measurement error of thermoEMF. The only device that uses a contact quality monitoring system is the SBA 458 NEMESIS device from the German company NETZSCH. The authors also encountered complaints about the manufactured thermoelectric control device “TERMOTEST-1”. Consumers noted low repeatability of results when taking multiple measurements of the same product. The analysis carried out by the authors showed that the low repeatability of the testing results was caused by high contact resistance with insufficient pressing force of the measuring electrodes to the test sample.

2. Problem statement

A thermoelectric monitoring device consists of an electronics unit and a sensor, which can be used for direct or differential measurement of thermoEMF. In the case of direct measurement of thermoEMF, the sensor consists of two electrodes: hot and cold (Fig. 1.a). For differential measurement of thermoEMF, the sensor must have two hot electrodes and two cold electrodes (Fig. 1.b).

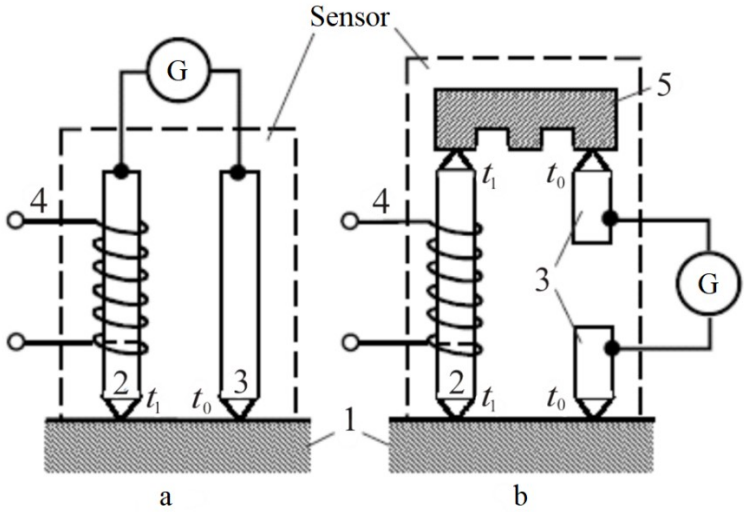

Fig.1. Sensor of a thermoelectric device, a – for direct measurement of thermoEMF, b – for differential measurement of thermoEMF, 1 – product under test; 2 – hot electrode; 3 – cold electrode; 4 – heater; 5 – standard sample (reference); G - galvanometer

The equivalent electrical circuit of the sensor for direct measurement of thermoEMF consists of contact thermoEMF E_1 and E_2, internal resistances of these thermoEMF R_1 and R_2, and contact resistances of each electrode R_3 and R_4 (Fig. 2). The current in the circuit (Fig. 2) will be determined by the internal resistance of the galvanometer, the internal resistances of the thermoEMF sources R_1 and R_2, and the contact resistances R_3 and R_4:

.

$$I = \frac{E_1 + E_2}{R_1 + R_2 + R_3 + R_4}.$$

The internal resistance of thermoEMF sources made of different materials can be in the range from 0.01 to 1 Ω. If the total contact resistance $R_c = R_3 + R_4$ changes from 0.01 to 100 Ω, then the thermoEMF source current will change by several orders. In practice, it is not the current that is measured, but the voltage; for this, instead of a galvanometer, a precision measuring resistor R_{ref} is used, on which the voltage resulting from the flow of current is measured. An equivalent circuit for this option is shown in Fig. 3, where E_1 – contact EMF of the hot electrode with an inspected sample, E_2 – contact EMF of the cold electrode with an inspected sample, R_1 – internal resistance of the contact EMF of the hot electrode with the inspected sample, R_2 – internal resistance of the contact EMF of the cold electrode with the inspected sample, R_3 – contact resistance of the hot electrode with the inspected sample, R_4 – contact resistance of the cold electrode with the inspected sample, G – galvanometer, R_c – total contact resistance, R_{ref} – measuring resistance.

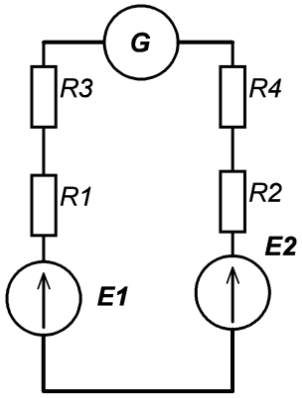

Fig.2. Equivalent electrical circuit of a thermoelectric sensor

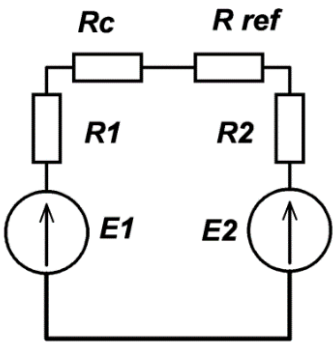

Fig.3. ThermoEMF measurement circuit

The voltage across the measuring resistor will be determined from the expression:

$$V = R_{ref} \frac{E_1 + E_2}{R_1 + R_2 + R_C + R_{ref}}.$$

The results of calculating the relative change in voltage across the measuring resistor when the total contact resistance R_c changes from 0.1 Ω to 10 kΩ for three resistances of the measuring resistor R_{ref} are shown in Fig.4. The internal resistance of the thermoEMF source was taken to be 0.1 Ω.

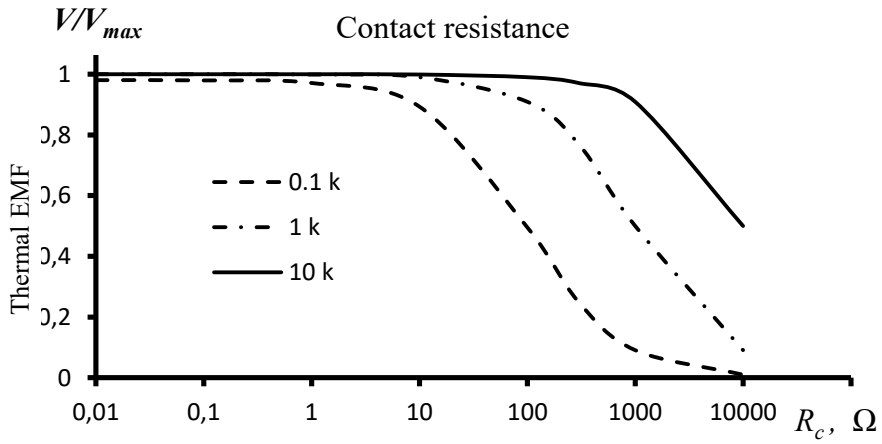

Fig.4. Dependence of the relative voltage across the measuring resistor on the total contact resistance for three measuring resistor values

From Fig. 4 it is clear that if a measuring resistor of 0.1 kΩ is used, the measured voltage will be 11% less than the true one with a 10 Ω contact resistance, and the measured voltage will be 50 % less than the true one with a 100 Ω contact resistance. If a 1 kΩ measuring resistor is used, then a 10 % decrease in measured voltage is observed for a 100 Ω contact resistance, and a 50 % decrease is observed for a 1 kΩ contact resistance. For a measuring resistance of 10 kΩ, a 10 % decrease in measured voltage is observed at a contact resistance of 1 kΩ. The permissible value of contact resistance, at which the measured thermoEMF value differs from the true value by no more than 10 %, should be no more than 9 Ω (measuring resistance 0.1 kΩ), 100 Ω (measuring resistance 1 kΩ) or 1 kΩ (measuring resistance 10 kΩ).

3. Method of Solution

Variations in contact resistance leads to variations in measurement results. To increase the reliability and repeatability of testing results, a contact resistance monitoring circuit is proposed. To do this, you can use an indirect method, which consists in measuring the voltage across the contact resistance thanks to the flow of a stable current. In order to find out the value of the total resistance of the contacts of the electrodes with the inspected product, a circuit shown in Fig. 5 was proposed.

The current from the generator flows through two circuits: through the measuring resistor R_{ref} and through series-connected resistors R_c+R_1+R_2. The equivalent load resistance for a stable current generator will be determined by the expression:

$$R_L = \frac{R_{ref} \cdot (R_C + R_1 + R_2)}{R_{ref} + R_C + R_1 + R_2}. \quad (1)$$

The results of the calculation using formula 1 of the dependence of the load resistance of the current generator on the contact resistance for three values of the measuring resistor are shown in Fig. 6. The following values were used in the calculation: R_1+R_2 = 0.1 Ω, R_{ref} = 0.1 kΩ; 1 kΩ; 10 kΩ.

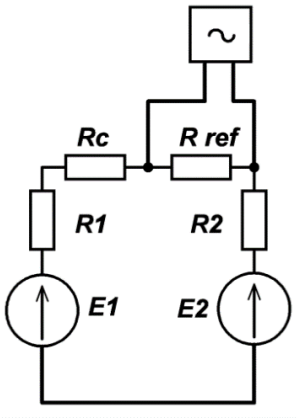

Fig.5. E Schematic diagram of the circuit used in the indirect measurement of the total contact resistance

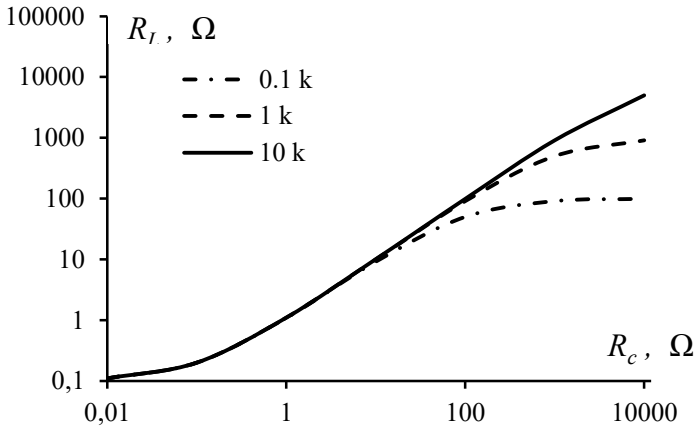

Fig.6. Dependence of the current generator load resistance on contact resistance

As can be seen from Fig. 6, with an increase in contact resistance, the load resistance of the stable current generator increases. At large values of contact resistance, it tends to the resistance of the measuring resistor. An increase in the load resistance of the current generator will lead to an increase in the voltage across the load, which will be determined by Ohm's law:

$$V_L = IR_L = I\frac{R_{ref} \cdot (R_C + R_1 + R_2)}{R_{ref} + R_C + R_1 + R_2}, \quad (2)$$

where I is the flowing generator current.

The modeling results of changes in the relative voltage across the load, performed in accordance with formula 2 for various values of the measuring resistance, are given in Table 1.

.

Table 1. Simulation results of relative voltage across the load

R_c, kΩ	$V_L/V_{L\,max}$		
	R_{ref} = 0,1 kΩ	R_{ref} = 1 kΩ	R_{ref} = 10 kΩ
0,01	0,00111	0,000121	2,19996E-05
0,1	0,002016	0,00022	3,9999E-05
1	0,010989	0,001209	0,000219975
10	0,092652	0,010999	0,002017952
100	0,505252	0,10009	0,019821487
1000	0,918189	0,550022	0,181833801
10000	1	1	1

The graphical dependence of the relative voltage across the current generator load on the contact resistance is shown in Fig. 7.

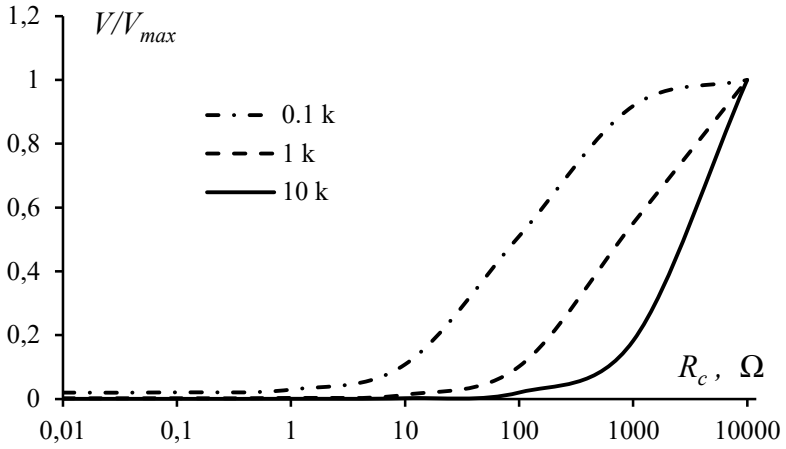

Fig.7. Dependence of the relative voltage on the load of the current generator on the contact resistance for three values of the measuring resistor

It is clear in Fig. 7 that if the contact resistance is less than 1 Ω, then the relative change in voltage across the load does not exceed 1% for a 0.1 kΩ measuring resistor and decreases by an order of magnitude for a 1 kΩ measuring resistor and by two orders of magnitude for a 10 kΩ measuring resistor. Taking into account the results presented in Fig. 4 for a contact resistance of 9 Ω (at R_{ref} = 0.1 kΩ), the relative change in voltage across the load of the current generator will be 10%, the same change will be for a contact resistance of 100 Ω (at R_{ref} = 1 kΩ) and 1 kΩ (at R_{ref} = 10 kΩ).

Connecting the current generator to the electrodes and determining the voltage at the contact resistance is explained in Fig.8. The current generator produces a sinusoidal current of constant amplitude I, independent of the load resistance. When this current flows through the measuring resistor, a voltage V_L appears. The same resistor is the load of the thermoEMF source and the voltage V_{EMF} is measured on it. Since V_{EMF} is a voltage with zero frequency, and V_L is a high-frequency voltage, then to separate these voltages, bandpass and band-stop filters with a resonant frequency equal to the frequency of the current generator are used.

From the output of the bandpass filter, the voltage is supplied to the amplifier, then to the rectifier, and to the analog-to-digital converter, from which the binary voltage code is sent to the microcontroller, which calculates the total contact resistance based on expression (4), after conversion of which we obtain

$$R_C = \frac{IR_{ref} \cdot (R_1 + R_2) - V_L(R_1 + R_2) - V_L R_{ref}}{V_L - IR_{ref}} \quad . \tag{3}$$

Taking into account the fact that $(R_1+R_2) << R_{ref}$, expression 3 simplifies to the form:

$$R_C = \frac{V_L R_{ref}}{IR_{ref} - V_L} = R_{ref} \frac{1}{\frac{IR_{ref}}{V_L} - 1}. \quad (4)$$

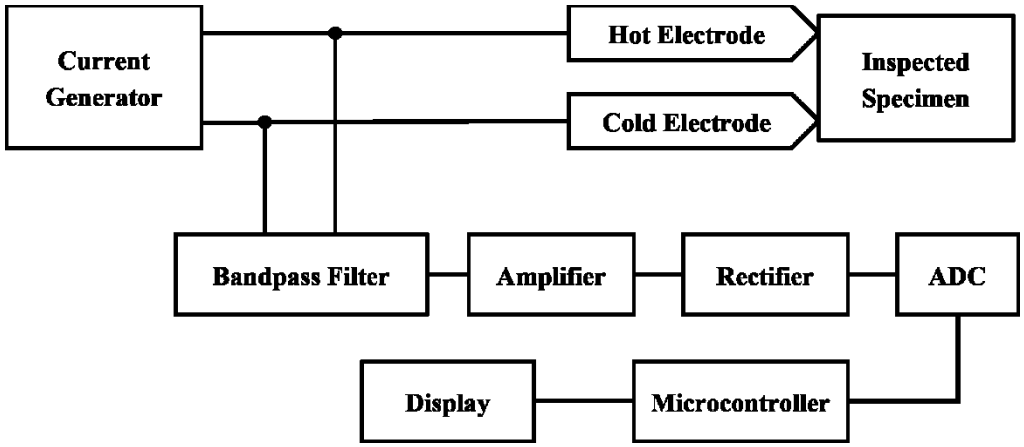

Fig.**8**. Block diagram of the control unit for the total contact resistance of the electrodes with the inspected product

The terms I and R_{ref} in expression (4) are constant quantities, therefore, to calculate the contact resistance it is necessary to measure only V_L. The proposed method allows you to check the value of the total contact resistance directly in the process of measuring thermoEMF.

4. Experimental Investigation

To conduct experimental studies, a stand was made containing an electronics module connected to a personal computer, a sensor and software that allows to display the value of thermoEMF and the total contact resistance (Fig. 9) [32]. The electronics module includes a system for heating and stabilizing the temperature of the hot electrode, a thermoEMF measurement system and a system for monitoring the total contact resistance. The measuring resistor in the experimental setup was 100 Ω with a tolerance of 1 %.

The hot electrode heating system and temperature stabilization system consist of Temperature Sensor 1, Temperature Sensor 2, heater, and microcontroller (Fig. 9). Information about the temperature of the hot electrode comes to the microcontroller from Temperature Sensor 1, and about the temperature of the cold electrode from Temperature Sensor 2. The microcontroller determines the temperature difference between the hot and cold electrodes and generates a control action for the heater to maintain the temperature difference between the hot and cold electrodes of 100 ºC.

The total contact resistance monitoring system consists of a high-frequency stable current generator, a bandpass filter, an amplifier, an AC voltage rectifier, an analog-to-digital converter (ADC2), and a microcontroller. A stable current generator produces an alternating current that flows through the contact resistance of the electrodes with the test sample. The voltage resulting from the flow of this current is isolated by a bandpass filter, amplified, rectified, and converted into a digital code that is sent to the microcontroller. The value of this voltage is used to determine the total contact resistance in accordance with formula (4).

The thermoEMF measurement system consists of a band-stop filter for suppressing the variable component, an amplifier, an analog-to-digital converter (ADC1) and a microcontroller. The voltage taken from the hot and cold electrodes, after suppressing the alternating component in the band-stop filter, is amplified, converted into a digital code and supplied to the microcontroller. The received information is transferred to a personal computer via the USB interface.

.

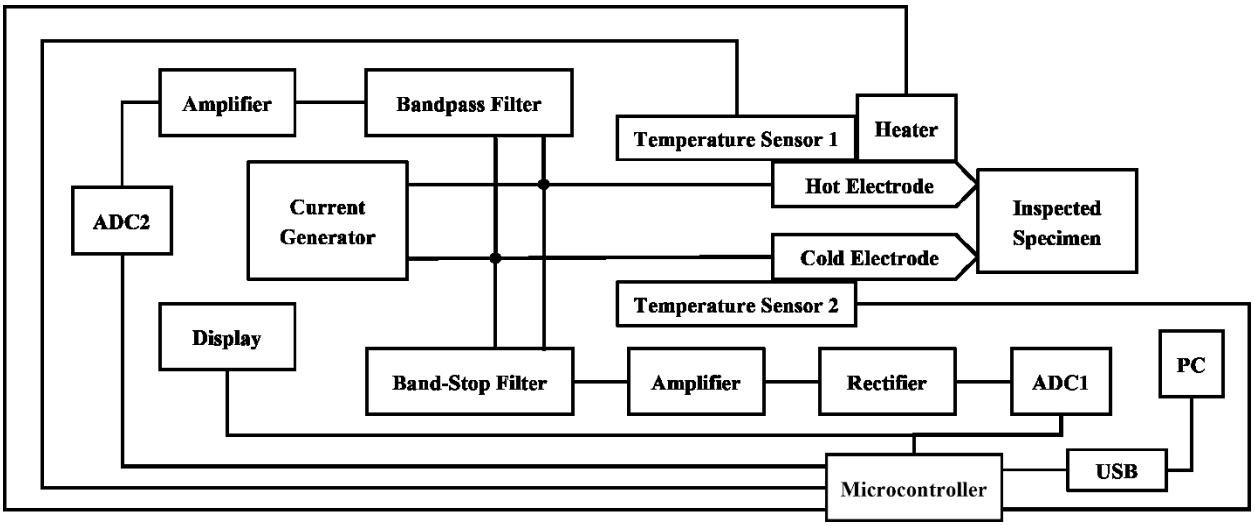

Fig.9. Structural diagram of the experimental installation

The computer software allows to display the obtained data in the form of a graphical dependence and save it in a separate file. The operator interface consists of two tabs (Fig. 10). The first tab is called "Charts" and allows to display data received continuously from the experimental setup. The second tab is called "Settings". This tab displays control data for the experimental setup (Fig. 11).

The "Charts" tab contains several windows. There is "Sum" at the top left of the window shown in Fig.10 displays the total thermoEMF value, and "Number of Values" displays the number of values involved in thermoEMF averaging, and "Average" displays the calculated average thermoEMF value. The next white box to the right shows the temperature of the hot electrode. The active tab shown in Fig. 10 contains two graphs. The top graph displays thermoEMF in green and contact resistance in red. Moreover, the scale of the axis for displaying contact resistance is reduced by 100 times, i.e. The displayed value must be increased by 100 times. The bottom graph displays thermoEMF in green and the temperature of the hot electrode in red, provided that the contact resistance is less than the set threshold value and the duration of this process is more than 1 second.

In order to explain the presented values in Fig. 10 and take them as an example, it is important to take into account that the x-axis of the top graph records time in 10 ms increments. The measurement process begins at a time corresponding to 2.2 s (count number 220). Until this time, the thermoEMF value is zero and the contact resistance is 4200 Ω, which corresponds to the maximum displayed value. In the reading interval 220…260, fluctuations in contact resistance up to 300 Ω are observed, the thermoEMF value is -20 μV. The calculated value is -18 μV. In the sampling interval of 280…300 and 320…340, the contact resistance is near zero, however, the measurement process was only 20 readings (200 ms), which is less than 1 second and therefore this data is not displayed in the lower graphic window. In the sampling interval 370…515, the contact resistance is about 10 Ω, the measurement process was 1.45 seconds. (515-370=145 counts), which is more than 1 second. and this interval is displayed in the lower window. From the bottom graph it can be seen that the temperature of the hot electrode is 132 ºC, and the thermoEMF is -69 μV. The graph shows a transient process that takes about 50 ms (counts from 0 to 5).

The "Settings" tab is used to control, manage and test the experimental setup (Fig. 11). The hot electrode heating system and temperature stabilization system consist of Temperature Sensor 1, Temperature Sensor 2, heater, and microcontroller (Fig. 9). Information about the temperature of the hot electrode comes to the microcontroller from Temperature Sensor 1, and about the temperature of the cold electrode from Temperature Sensor 2. The microcontroller determines the temperature difference between the hot and cold electrodes and generates a control action for the heater to maintain the temperature difference between the hot and cold electrodes of 100 ºC.

Fig.10. The developed computer software with the “Charts” tab on

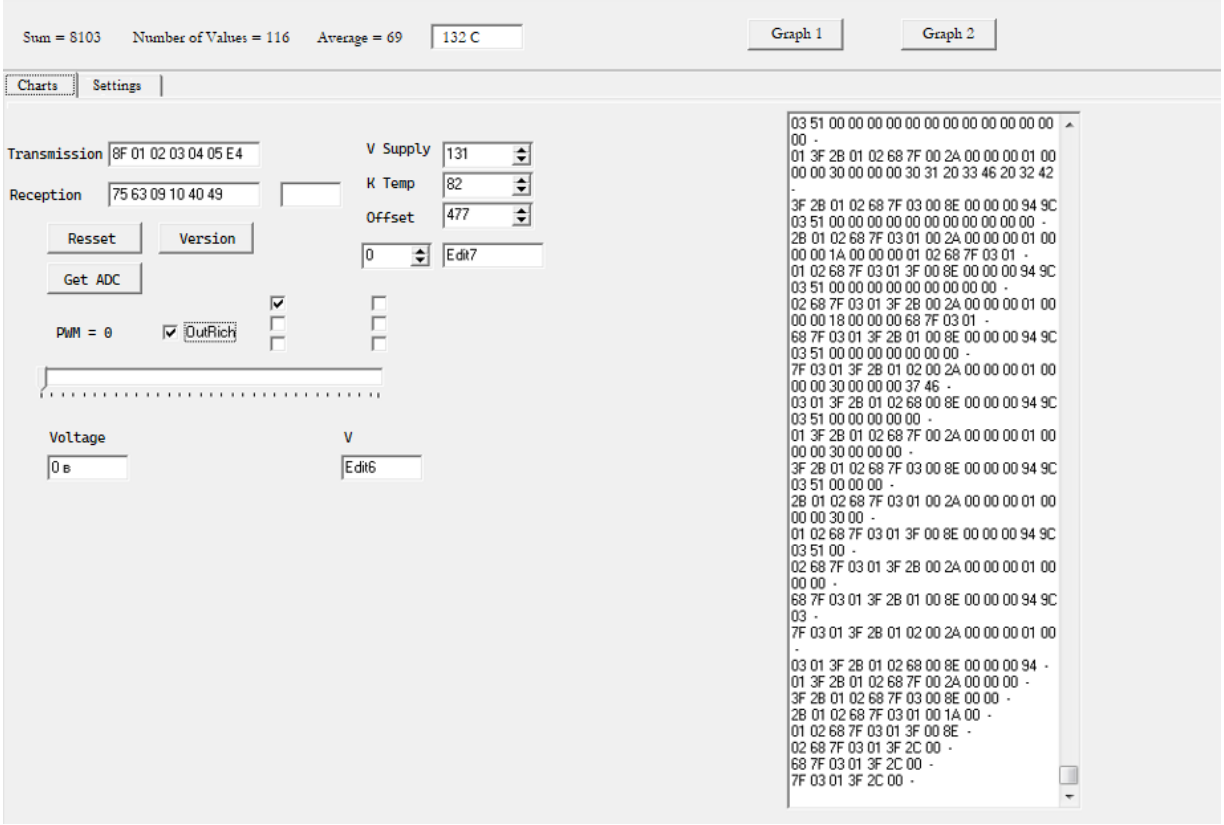

Fig.11. The developed computer software with the “Settings” tab on

The total contact resistance monitoring system consists of a high-frequency stable current generator, a bandpass filter, an amplifier, an AC voltage rectifier, an analog-to-digital converter (ADC2), and a microcontroller. A stable current generator produces an alternating current that flows through the contact resistance of the electrodes with the test sample. The voltage resulting from the flow of this current is isolated by a bandpass filter, amplified, rectified, and converted into a digital code that is sent to the microcontroller. The value of this voltage is used to determine the total contact resistance in accordance with formula (4).

The thermoEMF measurement system consists of a band-stop filter for suppressing the variable component, an amplifier, an analog-to-digital converter (ADC1) and a microcontroller. The voltage taken from the hot and cold electrodes, after suppressing the alternating component in the band-stop filter, is amplified, converted into a digital code and supplied to the microcontroller. The received information is transferred to a personal computer via the USB interface.

The “Reset” button allows to set the stand to its original state. The “Version” button allows you to display the name of the current version of the microcontroller program. The “Get ADC” button is used to check the operation of the analog-to-digital converter. The “V Supply” box displays supply voltage counts, whereas the “K temp” box shows a coefficient for calculating the temperature of the hot electrode. In the “Offset” window, you set the offset of the thermocouple characteristic for measuring the temperature of the hot electrode. The right window displays data coming from the test bench. The “Settings” tab is used during the initial setup of the experimental stand.

5. Conclusion

The conducted studies showed the influence of contact resistance on the result of inspection by the thermoelectric method. A method for monitoring contact resistance has been proposed and investigated, which consists of measuring the voltage across resistance when current flows from a high-frequency generator, which makes it possible to measure contact resistance directly in the process of monitoring thermoEMF.

The accuracy of measuring contact resistance depends on the accuracy of measuring the high-frequency voltage after rectification, which is determined by the ADC error and the quantization step. Modern microcontrollers have built-in ADCs, the quantization step of which is 2.5 mV, and the absolute error does not exceed 2 or 3 least significant digits of the ADC. In addition, the accuracy of the contact resistance measurement will be affected by the stability of the voltage and current of the high-frequency generator. In practical implementation, the total error in determining the contact resistance did not exceed 10%. The proposed method is advisable to use with manual testing devices when it is impossible to ensure the same pressing force of the sensor to the test sample during repeated measurements. In automated thermoEMF measurement systems, the clamping force is maintained the same in each measurement cycle and, in this manner, the potential for encountering this problem is eliminated. In the current case, the existing standards do not take into account the magnitude of contact resistance and are based on zero contact resistance. However, in the presence of contact resistance, the result of measuring thermoEMF will depend on the value of the contact resistance, which must be taken into account.

The proposed approach can provide a significant increase in the reliability of thermoelectric inspection results through the use of a contact resistance control unit and rejection of results with high contact resistance. The permissible value of contact resistance depends on the size of the measuring resistor and the internal resistance of the thermoEMF source. The larger the value of the measuring resistor, the greater the permissible value of contact resistance. The choice of acceptable value depends on the required accuracy of thermoEMF measurement. For a measuring resistor with a resistance of 1 kΩ, an internal resistance of the thermoEMF source of 0.1 Ω and an allowable value of contact resistance of 10 Ω, the thermoEMF measurement error caused by the contact resistance will not exceed 1%.

The proposed system for monitoring contact resistance was implemented in the thermoelectric testing device “TERMOTEST-2”, where the problem of low repeatability of testing results disappeared. If the contact resistance is more than 1 Ohm, the measurement result is not displayed on the device indicator and it is necessary to re-measure. It should be noted that the system for measuring contact resistance can be made in the form of an autonomous unit, which can be equipped with thermoelectric control devices in operation and thereby increase the reliability of the measurement results.

Conflict of interest statement

The authors declare that they have no conflict of interest in relation to this research, whether financial, personal, authorship or otherwise, that could affect the research and its results presented in this paper.

CRediT author statement

Kostina M.A.: Formal analysis, Data Curation; Soldatov A.I.: Conceptualization, Methodology, Project administration; Soldatov A.A.: Investigation, Validation; Abouellail A.A.: Software.
The final manuscript was read and approved by all authors.

References

1 Carreon H. (2002) Thermoelectric Nondestructive Evaluation of Residual Stress in Shot-Peened Metals. *Research in Nondestructive Evaluation*. 14(2), 59 – 80. DOI: 10.1080/09349840209409705.

2 Nagy P.B. (2010) Non-destructive methods for materials' state awareness monitoring. *Insight: Non-Destructive Testing and Condition Monitoring*. 52(2), 61 – 71. DOI: 10.1784/insi.2010.52.2.61.

3 Li J.F., Liu W.S., Zhao L.D., Zhou M. (2010) High-performance nanostructured thermoelectric materials. *Npg Asia Mater*. 2(4), 152 – 158. DOI: 10.1038/asiamat.2010.138.

4 Kikuchi M. (2010) Dental alloy sorting by the thermoelectric method. *European Journal of Dentistry*. 4(1), 66 – 70. Available at: https://www.ncbi.nlm.nih.gov/pmc/articles/PMC2798792/

5 Stuart C. (1987) Thermoelectric Differences Used for Metal Sorting. *Journal of Testing and Evaluation*. 15(4), 224 – 230. DOI: 10.1520/JTE11013J. ISSN 0090-3973.

6 Dragunov V.K., Goncharov A.L. (2019) New approaches to the rational manufacturing of combined constructions by EBW. *Proceeding of the IOP Conference Series: Materials Science and Engineering*. 681, 012010. DOI:10.1088/1757-899X/681/1/012010.

7 Goncharov A., Sliva A., Kharitonov I., Chulkova A., Terentyev E. (2020). Research of thermoelectric effects and their influence on electron beam in the process of welding of dissimilar steels. *Proceeding of the IOP Conference Series: Materials Science and Engineering*. 759(1), 012008. DOI: 10.1088/1757-899X/759/1/012008

8 Kharitonov I.A., Rodyakina R.V., Goncharov A.L. (2020) Investigation of magnetic properties of various structural classes steels in weak magnetic fields characteristic for generation of thermoelectric currents in electron beam welding. *Solid State Phenomena*. 299, 1201–1207. DOI: 10.4028/www.scientific.net/SSP.299.1201.

9 Soldatov A.I., Soldatov A.A., Sorokin P.V., Abouellail A.A., Obach I.I., Bortalevich V.Y., Shinyakov Y.A., Sukhorukov M.P. (2017) An experimental setup for studying electric characteristics of thermocouples. *SIBCON 2017 – Proceedings*. 79985342017. DOI: 10.1109/SIBCON.2017.7998534.

10 Carreon H., Medina A. (2007) Nondestructive characterization of the level of plastic deformation by thermoelectric power measurements in cold-rolled Ti–6Al–4V samples. *Nondestructive Testing and Evaluation*. 22(4), 299-311. DOI: 10.1080/10589750701546960

11 Carreon H. (2013) Detection of fretting damage in aerospace materials by thermoelectric means. *Nondestructive Characterization for Composite Materials, Aerospace Engineering, Civil Infrastructure, and Homeland Security*. 8694. DOI: 10.1117/12.2009448.

12 Lakshminarayan B., Carreon H., Nagy P. (2003) Monitoring of the Level of Residual Stress in Surface Treated Specimens by a Noncontacting Thermoelectric Technique. *AIP Conference Procceding*. 657, 1523-1530. DOI:10.1063/1.1570311.

13 Milićević I., Popović M., Dučić N., Slavković R., Dragićević S., Maričić A. (2018) Experimental Identification of the Degree of Deformation of a Wire Subjected to Bending. *Science of Sintering*. 50(2), 183-191. DOI:10.2298/SOS1802183M.

14 Soldatov A.I., Soldatov A.A., Sorokin P.V., Abouellail A.A., Kostina M.A. (2018) Thermoelectric method of plastic deformation detection. *Materials Science Forum*. 938, 112-118. DOI: 10.4028/www.scientific.net/MSF.938.112.

15 Magalhães A., De Backer J., Bolmsjö G. (2019) Thermal Dissipation Effect on Temperature-controlled Friction Stir Welding. *Soldagem & Inspeção*. 24(3), 1-9. DOI: 10.1590/0104-9224/si24.28.

16 Silva Ana C.F., De Backer J., Bolmsjö G. (2015) TWT method for temperature measurement during FSW process. *The 4th international conference on scientific and technical advances on friction stir welding & processing*. 95-98. Available at: https://www.diva-portal.org/smash/record.jsf?pid=diva2%3A1290065&dswid=554.

17 De Backer J., Bolmsjö G., and Christiansson A.-K. (2014) Temperature control of robotic friction stir welding using the thermoelectric effect. *The International Journal of Advanced Manufacturing Technology*. 70, 375-383. DOI:10.1007/s00170-013-5279-0.

18 Silva Ana C. F., De Backer J., Bolmsjö G. (2015) Cooling rate effect on temperature controlled FSW process. *Proceeding of the VII Intern. Conf. "High-Strength Materials: Challenges and Applications"*. Available at: https://www.researchgate.net/publication/281450403_Cooling_rate_effect_on_temperature_controlled_FSW_process.

.

19 Silva Ana C.F., De Backer J., Bolmsjö G. 2016. Analysis of plunge and dwell parameters of robotic FSW using TWT temperature feedback control. *Proceeding of the 11th Intern. Symposium on FSW*. Available at: https://www.researchgate.net/publication/303389476_ANALYSIS_OF_PLUNGE_AND_DWELL_PARAMETERS.

20 Vasiliev I., Soldatov A., Abouellail A., Kostina M.A., Soldatov A.A., Soldatov D., Bortalevich S. (2021) Thermoelectric Quality Control of the Application of Heat-Conducting Compound. *Studies in Systems, Decision and Control.* 351, 59–68. DOI: 10.1007/978-3-030-68103-6_6.

21 Yang Zhou, Donghua Yang, Liangliang Li, Fu Li, and Jing-Feng Li. (2014) Fast Seebeck coefficient measurement based on dynamic method. *Review of Scientific Instruments*. 85, 054904. DOI: 10.1063/1.4876595.

22 Uchida K., Ota T., Adachi H., Xiao J., Nonaka T., Kajiwara Y., Bauer G.E.W., Maekawa S., Saitoh E. (2012) Thermal spin pumping and magnon-phonon-mediated spin-Seebeck effect. *Journal of Applied Physics*. 111(10), 103903. DOI:10.1063/1.4716012.

23 Uchida K., Takahashi S., Harii K., Ieda J., Koshibae W., Ando K., Maekawa S., Saitoh E. (2008) Observation of the spin Seebeck effect. *Nature*. 455, 778–781. DOI: 10.1038/nature07321.

24 Lider A.M., Larionov V.V., Syrtanov M.S. (2016) Hydrogen concentration measurements at titanium layers by means of thermo-EMF. *Key Engineering Materials*. 683, 199 – 202. DOI: 10.4028/www.scientific.net/KEM.683.199.

25 Iwanaga S., Toberer E.S., LaLonde A., Snyder G.J. (2011) A high temperature apparatus for measurement of the Seebeck coefficient. *Review of Scientific Instruments.* 82(6), 063905. DOI: 10.1063/1.3601358.

26 Sarath Kumar S.R., Kasiviswanathan S. (2008) A hot probe setup for the measurement of the Seebeck coefficient of thin wires and thin films using integral method. *Review of Scientific Instruments.* 79, 02432, DOI: 10.1063/1.2869039.

27 Abouellail A.A., Chang J., Soldatov A.I., Soldatov A.A., Kostina M.A., Vasiliev I.M. (2023) Thermoelectric Monitoring Of Thermal Resistance In Electronic Systems. *Eurasian Physical Technical Journal*. 20(3), 52-61. DOI: 10.31489/2023No3/52-61.

28 Soldatov A.I., Soldatov A.A., Sorokin P.V., Loginov E.L., Abouellail A.A., Kozhemyak O.A., Bortalevich S.I. (2016) Control system for device «thermotest». *International Siberian Conference on Control and Communications (SIBCON-2016).* 1-5. DOI: 10.1109/SIBCON.2016.7491869.

29 Hu J., Nagy P.B. (1998) On the role of interface imperfections in thermoelectric nondestructive materials characterization. *Applied Physics Letters.* 73, 467-469. DOI: http://dx.doi.org/10.1063/1.121902.

30 Abouellail A.A., Chang, J., Soldatov, A.I., Soldatov, A.A.,.Kostina, M.A., Bortalevich, S.I., Soldatov, D.A. (2022) Influence of Destabilizing Factors on Results of Thermoelectric Testing. *Russian Journal of Nondestructive Testing*. 58(7), 607–616. doi.org/10.1134/S1061830922070026.

31 Sergeev A.S., Tikhonova Z.S., Uvarova T.V. (2017) Method for measuring thermo-emf of a "tool-workpiece" natural thermocouple in chip forming machining. *MATEC Web of Conferences*. 129, 01044. DOI: 10.1051/matecconf/201712901044.

32 Abouellail1 A.A., Kostina M.A., Bortalevich S.I., Loginov E.L., Shinyakov Y.A., Sukhorukov M.P. (2018) Mathematical simulation of thermocouple characteristics. *Proceeding of the IOP Conference Series: Materials Science and Engineering.* 327(2), 022002. DOI: 10.1088/1757-899X/327/2/022002.

AUTHORS' INFORMATION

Soldatov, Andrey Alekseevich – Candidate of techn. sciences, Associate Professor, National Research Tomsk Polytechnical University, Tomsk, Russia; ORCID ID: 0000-0003-0696-716X; soldatov.88@bk.ru

Soldatov, Aleksey Ivanovich – Doctor of techn. sciences, Professor, National Research Tomsk Polytechnical University, Tomsk, Russia, Tomsk, Russia; ORCID iD: 0000-0003-1892-1644; asoldatof@mail.ru

Kostina, Maria Alekseevna – Candidate of techn. sciences, Associate Professor, National Research Tomsk Polytechnical University, Tomsk, Russia; ORCID ID: 0000-0003-2626-6002; mariyakostina91@mail.ru

Abouellail, Ahmed Ali – Candidate of techn. sciences, Lecturer, Sphinx University, New Asyut, Egypt; ORCID iD: 0000-0002-9357-6214; ahmed.abouellail@sphinx.edu.eg